Test and optimization of timing algorithms for PET detectors with digital sampling front-end

Baptiste Joly, Gerard Montarou, J. Lecoq, G. Bohner, M. Crouau, M. Brossard, P.-E. Vert

Test and Optimization of Timing Algorithms for PET Detectors with Digital Sampling Front-end

B. Joly, *Member, IEEE,* G. Montarou, *Member, IEEE,* J. Lecoq, G. Bohner, M. Crouau, M. Brossard, P-E. Vert

***Abstract*—We tested a digital front-end concept in order to evaluate the time resolution of PET detectors based on APD or PMT with digital read-out. Measurements were done on a coincidence set-up with two detection blocks composed of a fast inorganic scintillator ($LaBr_3$ or LYSO) coupled to a photodetector (APD or PMT), preamplificators and prefilters. The signals were sampled at high rate (250MHz for APDs, 5GHz for PMTs) and treated offline. Two different timing algorithms were applied: a digital method deriving from constant fraction discriminator, and an optimal filtering technique based on parameter estimation with minimal variance. The classical optimal filter was adapted to the non-stationary noise conditions, with a significant improvement of timing resolution. We describe these algorithms and discuss their performances.**

I. Introduction

THE classical analog front-end circuits of gamma-ray detectors tend to be replaced by digital systems based on sampling with a free-running ADC and digital signal processing by programmable logic circuits (FPGA, DSP). In High Energy Physics, a digital read-out is used with various detectors for a better design flexibility, optimal energy and time resolutions.

In the context of the INNOTEP collaboration devoted to novel imaging systems for in-vivo monitoring during tumor ion beam therapy, we develop innovative electronics concepts for in-beam PET, with strong constraints on sensitivity, high bandwidth and time resolution. The architecture under study consists in a pixellated detector where each crystal is coupled to a compact photodetector, whose signal is read out by an electronic channel. The signal is prefiltered, sampled by a free-running ADC, and processed by programmable logic circuits (FPGA). The advantages of such architecture are: a high bandwidth, a parallel treatment of many pixel signals, a deadtimeless pipelined processing, potentially good energy and time resolutions, and design flexibility.

In this framework, we study an optimized algorithm for better time resolution. The interest of improving time resolution is manifold ([4], [5]). Firstly, the reduction of time resolution down to 1ns allows a reduction of coincidence time window to a value determined by the geometry of field-of-view. This leads to a better rejection of random coincidences. Secondly, a time resolution of some hundreds of picoseconds allows time-of-flight (TOF) measurement. The corresponding spatial information on the position of $\beta+$ emission along the line of response leads to a very significant reduction of noise variance in reconstructed image. Third, the TOF information allows faster reconstruction of activity distribution by segmentation methods. Finally, in the context of in-beam PET, an accurate timing of detected events allows time gating with the ion beam.

We compare two different timing algorithms: a Digital Constant Fraction Discriminator (DCFD), and an Optimal Filtering (OF) technique based on parameter estimation with minimal variance. Both algorithms can be described as linear filter based techniques, with different filters and underlying concepts. While DCFD algorithm is based on few samples for time measurement, the inputs of the OF algorithm are all the samples in the leading edge and some samples in the decaying part. Time and energy are estimated from two linear sums, with coefficients optimized with respect to the statistical properties of noise. Taking in consideration non-stationary noise leads to a significant improvement in time resolution.

The algorithms are tested on two experimental set-ups, one using APDs and the other using PMTs.

II. Description of the Algorithms

Both tested algorithms are based on the transformation of sampled signal s to a bipolar signal s_b by linear filtering. This filtered signal is then used to determine a time reference (zero-crossing time) independent of pulse amplitude. The bipolar signal s_b is defined at each step k as a linear sum of the n previous samples of the original signal:

$$s_b[k] = \sum_{i=1}^{n} b[i]s[k+i-n] \tag{1}$$

The set of n samples from $k+1-n$ to k used in the calculation can be defined as a vector S_k, and is equivalent to the content of a shift register recording the n previous samples. With B as filter coefficients vector, and $B^\top$ its transpose,(1) becomes in a matrix formulation:

$$s_b[k] = B^\top S_k \tag{2}$$

The filtered signal is computed only on a limited time interval. Indeed, it is useful to execute the calculation on a well chosen time interval to obtain some points around the zero crossing of filtered signal. This is achieved by a preliminary coarse timing procedure: the first sample above a threshold defines a time reference k_{ref}. The signal is stored on a time

Manuscript received November 14, 2008.

All authors are with the Laboratoire de Physique Corpusculaire de Clermont-Ferrand, 24 Avenue des Landais, 63177 Aubière Cedex, France (telephone: +334-73-40-73-13, e-mail: joly@clermont.in2p3.fr).

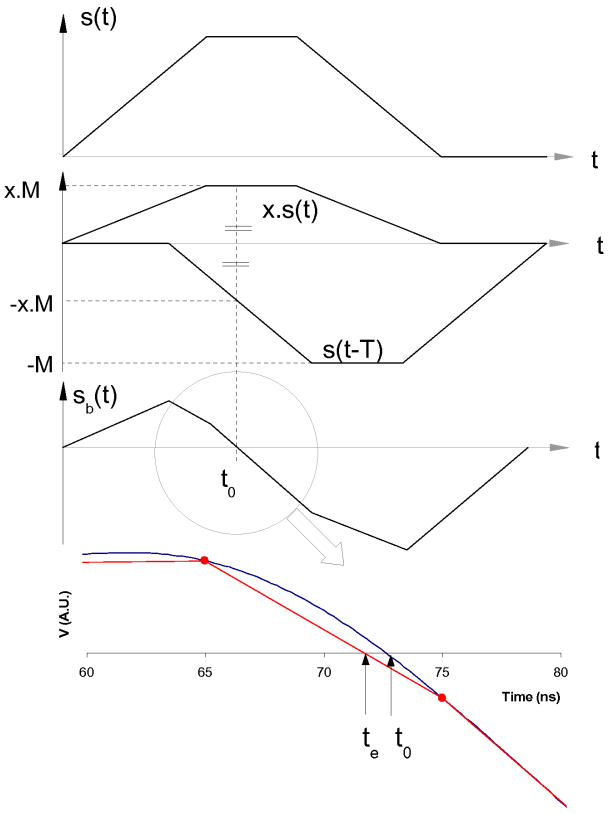

Fig. 1. Principle of constant fraction discriminator. *Top graph*: schematic detector pulse, *second*: attenuated and delayed-inverted versions, *third*: bipolar sum. The bipolar signal crosses the baseline when the delayed signal reaches a threshold equal to a fraction x of its maximum. Zero-crossing time is then independent of pulse amplitude. *Bottom graph*: estimation of zero-crossing time by linear interpolation. The difference between "analog" zero-crossing time t_0 and interpolated value t_e increases with sampling step and trace curvature.

interval $[k_{ref} - n_{pre}, k_{ref} + n_{post}]$ around the reference time. The resulting data will be referred to as "synchronized" pulse hereafter. If N samples are stored by the synchronization procedure, then $N - n + 1$ successive values of filtered signal should be calculated.

The algorithms differ by the choice of filter coefficients, and the zero-crossing time estimation technique.

A. Digital Constant Fraction Discriminator (DCFD)

By analogy with analog Constant Fraction Discriminator, the bipolar signal is built by a sum of two transformed versions of original signal: one is attenuated by a factor x, the other one is first delayed by a time T_d and then inverted.

$$s_b(t) = x\, s_a(t) - s(t - T_d) \tag{3}$$

The resulting bipolar pulse crosses the baseline at time t_0, when the original signal reaches the fraction x of its maximum on the rising edge. The resulting time at zero-crossing is thus independent of pulse amplitude.

In the context of digital processing, the same transformation can be applied if the delay T is a multiple of sampling period. We thus write

$$s_b[k] = x\, s[k] - s[k - T] \tag{4}$$

In the formalism of (1), only two filter coefficients are nonzero:

$$b[n] = x \quad \text{and} \quad b[n - T] = -1 \tag{5}$$

The calculation of each filtered sample is then reduced to a multiplication and a subtraction. Because of this feature, the algorithm is interesting for FPGA implementation.

Once the last positive sample of s_b and the first negative one have been identified, the time at zero-crossing is estimated by linear interpolation as shown Fig.1.

At moderate sampling rate, an error is introduced by curvature. As this error is related to signal phase with respect to the sampling clock, the interpolated time can be corrected by look-up table based methods.

B. Optimal Filter (OF)

The optimal filtering is an algorithm that can be used to reconstruct time and amplitude of an analog signal from its digital samples. This method had been extensively used in High Energy Physics for LHC calorimeter signal processing. ([8], [7], [9],[15])

The pulse shape is assumed to be reproducible and thus known with good precision. The latter is described by a function $g(t)$ starting at $t = 0$ with an amplitude normalized to 1. We thus assume that each synchronized pulse can be approximated by

$$s[i] = a\, g\big(i\, T_s - t_0\big) \tag{6}$$

where a is the amplitude, T_s the sampling period and t_0 the time shift between sampling clock and the event starting time, *i.e.* a time related (*via* a constant delay) to the instant of gamma interaction in the crystal. As the positrons are emitted at random times, t_0 is uniformly distributed between 0 and T_s. A typical case is shown Fig. 2 to illustrate the parameters definition.

If the time shift t_0 is small, the reference shape function $g(t)$ can be linearly approximated,

$$g(i\, T_s - t_0) \approx g(i\, T_s) - t_0 g'(i\, T_s) \tag{7}$$

By substitution in (6):

$$s[i] \approx a g(i\, T_s) - a\, t_0 g'(i\, T_s) \tag{8}$$

This relation is written is matrix form:

$$S \approx aG - a\, t_0 G' \tag{9}$$

where

$$G = \begin{pmatrix} g(0) \\ g(T_s 0) \\ \vdots \\ g\big((n-1)\, T_s\big) \end{pmatrix} \tag{10}$$

and

$$G' = \begin{pmatrix} g'(0) \\ g'(T_s 0) \\ \vdots \\ g'\big((n-1)\, T_s\big) \end{pmatrix} \tag{11}$$

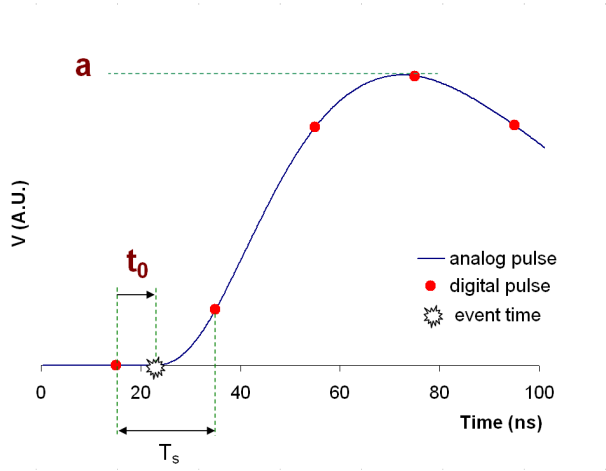

Fig. 2. Illustration of amplitude a and time shift t_0 to be reconstructed by the optimal filter algorithm. t_0 is the time shift between sampling clock and the event time. The latter is related to the instant of gamma interaction in the crystal.

We determine two coefficient vectors A and B, verifying the orthogonality conditions,

$$A^\top G = 1 \quad (12)$$
$$A^\top G' = 0 \quad (13)$$
$$B^\top G = 0 \quad (14)$$
$$B^\top G' = -1 \quad (15)$$

Then the parameters will be estimated by two weighted sums: u is the estimator of amplitude a and v the estimator of the product of amplitude and time, at_0.

$$u = A^\top S \quad (16)$$
$$u \approx a \quad (17)$$
$$v = B^\top S \quad (18)$$
$$v \approx at_0 \quad (19)$$

The computation of amplitude and time is based on two weighted sums, and a division to extract t_0. Because of its relative simplicity, the method is particularly appropriate for FPGA implementation.

Note that the estimators u and v can be considered as samples extracted from two filtered signals: the amplitude a corresponds to the maximum of u and the time t_0 to the zero-crossing time of v. This is why the method is named here "filtering", although it should be more adequately defined as a fit technique.

As the reconstruction of t_0 is based on a local linearization, the same curvature error than mentioned for DCFD time interpolation exists. This error increases with sampling step and signal curvature, and the reconstructed time can be corrected by the same technique, or by using several coefficient vectors as in [8].

The coefficients are not completely constrained by the orthogonality relations (12) to (15). Among all the coefficient vectors verifying these relations, we want to determine those which are optimal for the given noise conditions.

III. Optimal weights

Measurements of amplitude and time are affected by statistical errors due to noise in the detector and the readout electronics. If the statistical properties of noise are known, the weight vectors A and B can be chosen to minimize the resulting error.

In this section, we write $< x >$ the mean value of the random variable x. The covariance matrix of a random vector X is the symmetric matrix

$$R_X = < XX^\top > - < X >< X >^\top \quad (20)$$

The (i, j) term of R_X is

$$r_{ij} = cov(x_i, x_j) = < x_i x_j > - < x_i >< x_j > \quad (21)$$

If N is a random vector describing a white noise, the successive samples are uncorrelated, and then R_N is a diagonal matrix.

A. Mathematical optimum

1) Variance of reconstructed parameters: We consider a set of pulses with defined amplitude a and having the same time origin t_0 with respect to sampling clock. The reconstructed parameters should be constant. However, due to noise and signal shape variation, they will fluctuate. We want to quantify and minimize the variance of these fluctuations.

We reformulate signal vector, adding a noise component to (9)

$$S = aG - at_0 G' + N \quad (22)$$

where N is vector of noise samples, with mean value equal to 0.

The errors on u and v are respectively:

$$\delta u = u - a = A^\top N \quad (23)$$
$$\delta v = v - at_0 = B^\top N \quad (24)$$

The variance of u is thus

$$var(u) = < (A^\top N)^2 > \quad (25)$$
$$= A^\top < NN^\top > A \quad (26)$$
$$= A^\top R A \quad (27)$$

where R is the covariance matrix of noise.

In a similar way, the variance of v is

$$var(v) = B^\top R B \quad (28)$$

The optimal weights are determined by minimizing $var(u)$ and $var(v)$ while respecting the orthogonality relations (12) to (15).

2) minimization techniques: This minimization is usually obtained by the Lagrange transformation method, which leads to a linear system. See [7] and [8] for details.

However, when the optimal filtering technique is applied to signal vectors with a large number of samples, the linear system can be illconditioned. This is especially true when the sampling step T_s is smaller than the noise correlation time. Indeed, this leads to a covariance matrix R with small variation between successive lines (or columns), and then with a small

determinant. The inversion of linear system is then affected by numerical errors.

To apply the OF technique in the above mentioned conditions, we employed a classical iterative minimization algorithm based on gradient descent with constraints to approach the minimum by successive steps.

B. Practical optimization from experimental data

The determination of optimal coefficients requires the knowledge of the covariance matrix R of noise. Photodetector signals are characterized by an intrinsic fluctuation, which appears as a non-stationary shot noise source. This fluctuation is a result of the random scintillation and photodetection processes.

We could calculate the N vectors from individual traces by normalization in amplitude, synchronization, and subtraction of the mean trace. The covariance matrix would then be calculated by the observed covariances

$$R_N =< NN^\top > \tag{29}$$

However, such a computation would be biased by the residual fluctuation of time origin t_0. As t_0 is uniformly distributed in $[0, T_s]$, the extra contribution on covariance matrix cannot be neglected.

To solve this problem, we modify the coefficient optimization technique. We work on a pair of detectors measuring coincident gammas from a punctual positron source equally distant from each detector. The signals are sampled simultaneously on a pair of channels (1 and 2). The indices 1 and 2 will refer to the respective channels hereafter. Instead of minimizing $var(v)$ on each channel, we minimize $var(\Delta t)$, where Δt is the difference between reconstructed times on the two channels:

$$\Delta t = v_1/u_1 - v_2/u_2 \tag{30}$$

As long as the pair of detected gammas is a true coincidence, the gamma interaction times are equal ($t_1 = t_2$), and the difference of reconstructed times between the two channels is not affected by the random character of emission times, but only by timing resolution.

We assume that a large number of coincident pairs of signals have been measured and stored. The pulses of both channels are synchronized with the same reference time, measured on channel 1. Each resulting trace is written S_i (for channel i). The sampled and synchronized pulse (here channel 1) is still approximated as (22):

$$S_1 = a_1 G_1 - a_1 t_1 G'_1 + N_1 \tag{31}$$

In this context, amplitude a_1 and time origin t_1 are random variables following some law: the amplitude a_1 fluctuates according to the detector energy resolution, and t_1 is at best uniformly distributed in $[0, T_s]$. For mathematical convenience, we assume $< t_1 >=< t_2 >= 0$, which can be obtained by an adequate choice of time origin.

Moreover, the shape function is now defined and calculated as the average pulse,

$$G_1 =< S_1 > \tag{32}$$

and G'_1 is its derivative calculated numerically.

As the signals are measured simultaneously, and assuming that all events are true coincidences, we have by definition

$$t_1 = t_2 \tag{33}$$

In a first step, the coefficients for energy estimation are optimized so as to minimize $var(u_1)$ and $var(u_2)$.

The variance of u_1 is given by:

$$\begin{aligned} var(u_1) &= var(A^\top S_1) && (34)\\ &= A_1^\top R_1 A_1 && (35) \end{aligned}$$

The matrix R_1 is the covariance matrix of measured signal S_1

$$R_1 =< S_1 S_1^\top > - < S_1 >< S_1 >^\top \tag{36}$$

Once the A_1 and A_2 vectors have been determined, the amplitudes u_1 and u_2 are estimated and each signal vector is normalized by its respective amplitude.

$$S_1^* = S_1/u_1 \tag{37}$$

Then, we can write, in good approximation:

$$S_1^* \approx G_1 - t_1 G'_1 + N_1^* \tag{38}$$

This normalization allows to minimize $var(\Delta t)$:

$$\begin{aligned} var(\Delta t) &= var(B_1^\top S_1^* - B_2^\top S_2^*) && (39)\\ &= var(B_{12}^\top S_{12}) && (40) \end{aligned}$$

Where B_{12} and S_{12} are built by a concatenation of respectively $(B_1\ ,\ B_2)$ and $(S_1^*\ ,\ -S_2^*)$, *i.e.*:

$$B_{12} = \begin{pmatrix} B_1 \\ B_2 \end{pmatrix} \tag{41}$$

$$S_{12} = \begin{pmatrix} S_1 \\ -S_2 \end{pmatrix} \tag{42}$$

Finally:

$$var(\Delta t) = B_{12}^\top R_{12} B_{12} \tag{43}$$

$$R_{12} =< S_{12}^\top S_{12} > - < S_{12}^\top >< S_{12} > \tag{44}$$

Where R_{12} is the covariance matrix of normalized dual channel signal vector S_{12}.

With this technique, the coefficients for time measurement are thus optimized simultaneously on a pair of channels. It is well adapted to a simple experimental context. For a whole detector composed of a large number of channels, an offline calibration procedure must be defined. For example, the optimal filter coefficients can be determined once for a particular pixel, and thereafter applied to all pixels assuming identical noise properties.

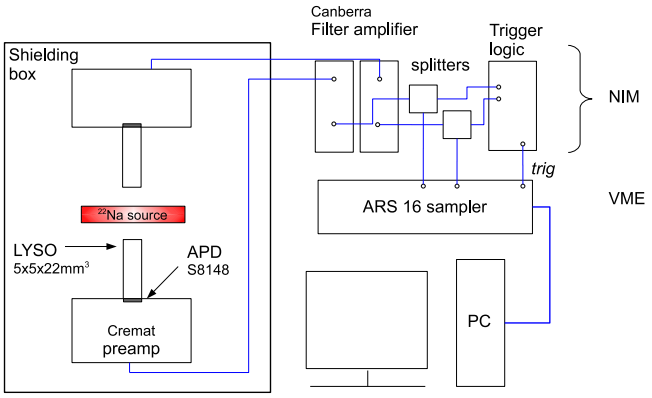

Fig. 3. Schematics of the experimental set-up for APD detectors

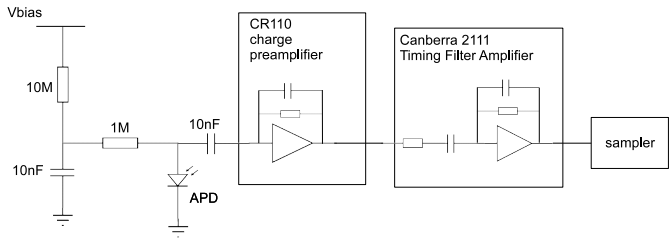

Fig. 4. Schematics of the APD read-out electronics

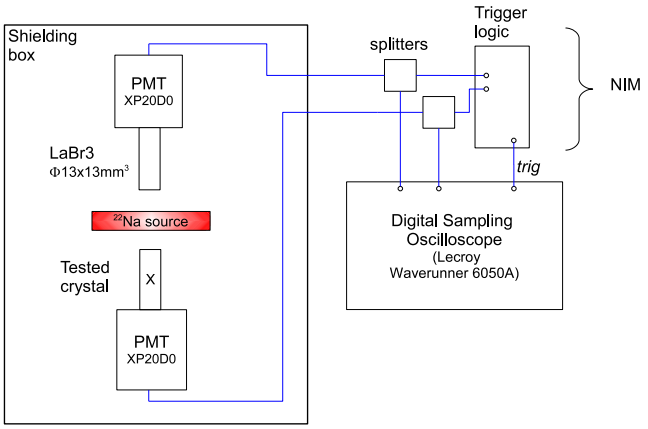

Fig. 5. Schematics of the experimental set-up for PMT detectors

IV. Experimental testing

Two series of tests were performed. The first one was dedicated to APD based detectors, and the second one to crystal comparison to optimize geometry and wrapping, using fast PMTs. The principle is the same in both cases. A ^{22}Na β^+ source is placed between two detectors, whose signals are digitized and stored when a coincidence is detected by the trigger logic. A splitter distributes the signal to trigger logic and to the sampling device. The detectors and preamplification electronics are placed in a large steel box for electromagnetic shielding and protection against ambient light. The difference between the two configurations lies in photodetector and read-out electronics.

A. APD set-up

Both detectors are composed of a 5x5x22mm^3 PreLude™ LYSO crystal from St Gobain Crystals, glued to a S8148 APD from Hamamatsu.

LYSO scintillator is a good candidate for PET ([17], [18]) due to its high density (7.1g/cm^3) and high photofraction, its fast decay (41ns) and good light yield (32 photons/keV). The mechanically polished crystals were wrapped with several layers of white Teflon tape as light reflector on 5 faces. The crystal was glued to the 5x5mm^2 active area of the APD. Both the APD and the wrapped crystal are embedded in a plastic protective box.

The S8148 APD is a "reverse" structure APD developed by Hamamatsu Photonics in collaboration with CMS for the electromagnetic calorimeter [27]. It was designed to be operated in a high radiation level with strong reliability constraints.

The advantages of the "reverse" structure compared to the older "reach through" type are fast response, good efficiency for visible light, low excess noise factor, moderate temperature dependence and radiation hardness. The S8148 APD shows a quantum efficiency of 75% at the PreLude maximum emission wavelength (420nm). Its excess noise factor is 2 at gain 50.

Each APD is connected to a Cremat CR110 charge sensitive preamplifier circuit shielded in aluminum housing. Cremat CR110 is a single channel, low noise charge sensitive preamplifier designed for various types of radiation detectors including PMTs and APDs. See Fig. 4 for a schematics of the APD front-end electronics.

The preamplifier output signal is driven to a NIM Canberra 2111 Timing Filter Amplifier for amplification and shaping. The integration and differentiation constants can be controlled on a wide range between 10ns and 500ns. Gain can be adjusted to fit the sampler dynamics. The filtered signals are sampled by a custom VME Analog Ring Sampler (ARS16) [32] with a sampling rate set to 250MHz and a 12 bit ADC resolution. The acquisition PC is connected to the VME crate via a USB interface module.

The APDs were biased at three different voltages, and the corresponding gain values were estimated by a method described in appendix A.

B. PMT set-up

The set-up is composed of two detectors based on a scintillator coupled to a Photonis XP20D0 PMT. The crystal channel 1 is a BrilLanCe™ $LaBr_3$ ϕ13x13mm^3 from St Gobain Crystals. $LaBr_3$ shows good timing properties due to its high light yield (63 ph/keV) and short decay time constant (16ns). For this reason, $LaBr_3$ is also a good candidate for PET ([21], [22]) although with some disadvantageous counting properties (density 5.29, low photofraction).

The channel connected to the detector with $LaBr_3$ is set as a reference channel (ch1). The detector crystal on the other channel (ch2) is the tested PreLude. Each crystal is coupled to the PMT silica window via silicone grease (Rhodorsil Silicone Pate 7). The tested crystal is mechanically maintained (when coupled to the PMT on the small square face) or simply stabilized by grease (when coupled on a long rectangular face). The most interesting tested crystal configurations are listed in Table I. Many other configurations were experimented, but the

TABLE I
PRELUDE CRYSTALS: GEOMETRY AND SURFACE

number	size(mm^3)	coupled face (mm^2)	wrapping
P1	2x2x10	2x10	white painting
P2	4x4x22	4x22	white painting
P3	5x5x22	5x5	Teflon tape
P4	10x10x10	10x10	Teflon tape

problem of scintillator optimization is well documented ([17], [18], [19], [22]) and is out of the scope of this paper.

The PMT anode outputs are connected to the 50Ω inputs of a Lecroy Waverunner 6050A digital oscilloscope with 500MHz bandwidth, sampling rate set to 5GS/s, and 8-bit conversion.

C. Data acquisition

A trigger signal is built from a coincidence of logic signals produced by constant fraction and leading edge discriminators. It corresponds to the detection of two pulses, with selected amplitude between high and low thresholds. The coincidence signal is synchronous with channel 1, with a jitter reduced by the use of constant fraction discriminators. The sampler reads the signals simultaneously on both channels and stores a pair of pulses on each trigger signal. 10000 pairs of pulse traces are stored for each test.

D. Offline data processing

The pairs of pulses are processed to calculate the average pulse and the dual channel covariance matrix as described above (III-B). The reference time for pulse synchronization is determined by DCFD algorithm.

Two pairs of coefficient vectors for timing are determined. The first one is optimized for a white stationary noise model, and the second one for the observed noise statistics. The OF algorithm using the respective coefficients is referred to as OF1 and OF2 hereafter.

The reconstructed time difference between the two channels is histogrammed, and the spectrum is fitted by a gaussian to estimate the standard deviation and the corresponding fwhm coincidence resolution. The spectrum width can also be measured on the histogram, and the result is consistent with gaussian fit with a maximal 4% difference.

V. RESULTS AND DISCUSSION

The results are listed in Table II for APD tests and in Table III for PMT measurements.

In Table IV, the coincidence resolution measured on the PMT tests is extrapolated to the context of two identical detectors, with the tested PreLude crystal, on both channels. This is calculated by subtracting in quadrature the measured contribution of channel 1 and applying the factor $\sqrt{2}$ to consider a pair of channels identical to ch2.

TABLE II
RESULTS WITH APD-BASED DETECTORS

gain	shaping time constant (ns)	Δt fwhm (**ns**)		
(estimated)	differentiate=integrate	DCFD	OF1	OF2
100	10	1.60	2.04	1.56
200	10	1.31	2.07	1.26
400	10	1.62	2.83	1.38
200	100	2.16	3.42	2.04

TABLE III
RESULTS WITH PMT-BASED DETECTORS

tested	light collection	energy	Δt fwhm (**ns**)		
crystal	(%$LaBr_3$)	resolution(%)	DCFD	OF1	OF2
$LaBr_3$	100	3.5	0.245	0.290	0.202
P1	41	12.3	0.317	0.433	0.255
P2	44	10.4	0.326	0.439	0.279
P3	37	11.1	0.353	0.492	0.297
P4	43	11.5	0.344	0.468	0.286

TABLE IV
COINCIDENCE TIME RESOLUTIONS WITH 2 X CRYSTAL B

tested	Δt (**ns**)		
crystal	DCFD	OF1	OF2
P1	0.375	0.539	0.299
P2	0.391	0.549	0.339
P3	0.435	0.632	0.368
P4	0.420	0.595	0.350

A. Performance comparison

In each configuration, the algorithms can be sorted by order of increasing performance: OF1, DCFD, OF2. In some APD configurations, the improvement from DCFD to OF2 is not significant. Generally, the gain is in the range 2-15% for APD signals and 13-20% for PMT signals. This low difference indicates that the DCFD method, based on the early rising edge, is close to optimal if threshold value is adjusted.

On the contrary, the improvement between OF1 and OF2 is always very significant, in the range 23-51%, which means that the actual noise properties must be considered for a correct optimization of timing coefficients.

The APD tests results indicate the existence of some optimal gain value around 200. The PMT tests show a strong correlation between light collection and time resolution. The crystal geometry also determines the rise time of light signal - increasing with photon transit time spread - which in turn influences timing resolution [17] [26].

B. DCFD: threshold optimization

We observe a strong dependence of timing resolution on the DCFD relative threshold x.

The relation between timing resolution and DFCD relative threshold (x) is plotted in Fig. 6 in the case of APDs operated at the optimal gain (approx. 200). The contribution of stationary noise is estimated by a comparison between the time resolutions of DCFD applied to the acquired pulses,

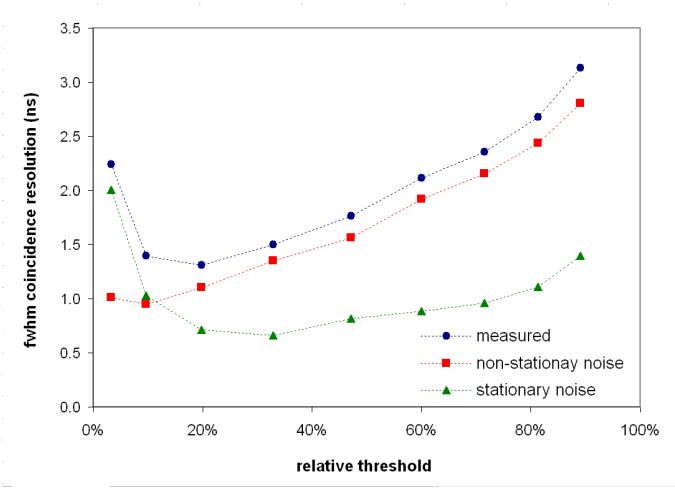

Fig. 6. Resolution of DCFD algorithm depending on relative threshold (fraction x) for APD signals: measured resolution (blue), estimated contributions of stationary (green) and non-stationary (red) noises.

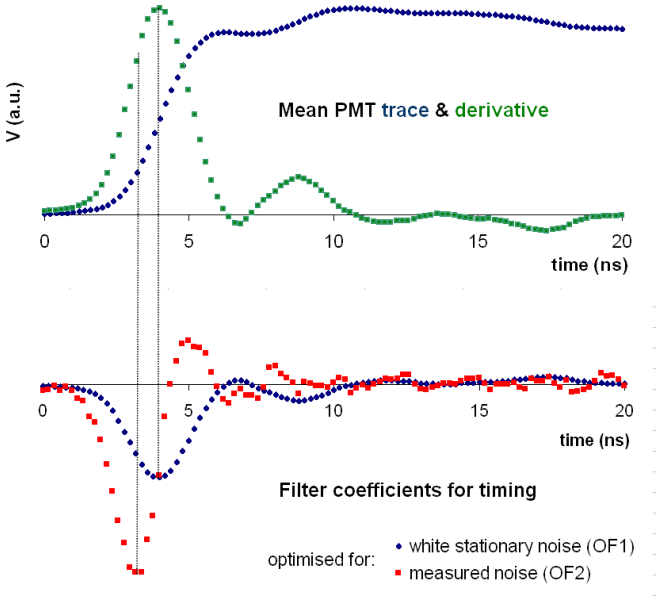

Fig. 7. Mean trace, its derivative, and timing weight coefficients (B_2) for OF1 and OF2, on channel 2. Coefficients optimized for white and stationary noise (OF1) are proportional to signal slope, while coefficients optimized for measured fluctuation (OF2) give more weight to the earlier part of rising edge.

and then to the sum of pulses and measured noise traces. The quadratic difference is assumed to be a good estimation of stationary noise contribution to the reconstructed times spread. The difference between stationary noise contribution and measured resolution is attributed to non-stationary noise. The contribution of the latter is thus also calculated by quadratic difference.

The time dispersion is fastly decreasing when threshold increases from 5%, and is dominated by the stationary noise component. After some optimal threshold value around 20%, the measured time dispersion increases faster than the contribution of stationary noise, and becomes dominated by non-stationary noise contribution.

The optimal threshold is thus determined by the relative importance of stationary and non-stationary noises, and is lower than the threshold corresponding to the maximal slope on the rising edge.

The optimal threshold value for APD signals at gains 100, 200, 400, and with 10ns shaping time constant, are respectively around 20%, 15%, 10%. The optimum is around 10%-15% for PMT signals.

The decrease of optimal threshold with APD gain is explained by the improvement of signal to stationary noise ratio (signal amplitude increases) and the degradation of signal to non-stationary noise ratio (excess noise factor increases with gain).

C. OF: coefficient optimization

The coefficient vectors of the OF1 and OF2 algorithms are plotted Fig. 7 with the average trace.

The coefficients optimized for white stationary noise (OF1) are proportional to signal slope, while those optimized for measured fluctuation (OF2) give maximal weight to the first part of rising edge, as the noise to slope ratio is minimal.

This also explains the small difference between the performances of DCFD and OF2 algorithms: both are based on a few samples in the early rising edge of detector signal.

VI. Conclusion

We adapted a timing algorithm based on optimal filtering (OF) to the specificity of PET detector signals, and compared its performance to an algorithm based on constant fraction discrimination (DCFD). We developed a method to adapt the linear filter to given signal shape and complex noise statistics by empirical data analysis on a pair of channels. Adapting the filter to the actual noise (OF2) instead of a simplified white stationary noise model (OF1) leads to a 23%-51% improvement in timing resolution. The performance of optimal filter (OF2) is up to 20% better than DCFD algorithm in the tested configurations.

Work is ongoing to study the effect of analog shaping and sampling frequency on achievable time resolution. The experimental tests will also be continued with fast compact photodetectors: MCPPMT and SiPM.

APPENDIX A
APD GAIN ESTIMATION

The 511keV photopeak amplitude V_{pp} was measured as a function of high voltage bias. This amplitude is related to APD gain via an unknown factor $V_{pp} = fM$, which is determined by scaling the relative gain curve with data published by Deiters [27] for the S8148 APD. The relative gain change coefficient $1/M \cdot dM/dV$ increases with gain following a linear law. By regression on Deiter's curve, we determined the coefficients

$$1/M \cdot dM/dV(V^{-1}) = 2.88 \times 10^{-4} M + 1.56 \times 10^{-2} \quad (45)$$

By regression on our measured data, we obtain

$$\begin{aligned} 1/M \cdot dM/dV(V^{-1}) &= 2.22 \times 10^{-4}(f(mV)M) \\ &\quad +1.48 \times 10^{-2} \end{aligned} \quad (46)$$

By identification, we determine the gain to amplitude factor $f = 1.30mV$ and the peak amplitudes in each configuration gives approximately the corresponding gain, with a precision estimated to 15% from the dispersion of measured points around the regression line.

REFERENCES

[1] P-E. Vert et al., "Contribution of HEP electronics techniques to the medical imaging field", Proceedings of the Euromedim, 1st European Conference on Molecular Imaging Technology, 9-12 May 2006, Marseille, France.

[2] P-E. Vert et al., "Innovative electronics architecture for PET imaging", IEEE NSS Conference Record, Vol.5, pp. 3057-3059, 2006.

[3] B. Joly, G. Montarou, N. Pauna, "First order simulations on time measurement using inorganic scintillators for PET Applications", IN2P3 Research report 1-37, http://hal.in2p3.fr/in2p3-00260869/en/, 2007

[4] W.W.Moses, "Time Of Flight PET revisited", IEEE Trans. Nucl. Sci., Vol. 50, pp. 1325-1330, 2003.

[5] Maurizio Conti, "Effect of randoms on signal-to-noise ratio in TOF PET", IEEE Trans. Nucl. Sci., Vol. 53, no. 3, pp. 1188-1193, 2006.

[6] A. Fallu-Labruyere, H. Tan, W. Hennig et W.K. Warburton, "Time resolution studies using digital constant fraction discrimination", Nucl. Instr. Meth. A, Vol. 579, pp.247-251, 2007

[7] E. Fullana et al. "Optimal filtering in the ATLAS hadronic tile calorimeter", Atlas internal note ATL-TILECAL-2005-001, 2005

[8] F. Camarena, J. Castelo, E. Fullana, "Optimal filtering applied to 1998 test beam of module 0", Atlas internal note ATL-TILECAL-2002-015, 2002.

[9] R. Brunelière, "CMS electromagnetic calorimeter performance and test beam results", Nucl. Instr. Meth. A, Vol. 572, pp 33-35, 2007

[10] A. Bousselham and C. Bohm, "Sampling pulses for optimal timing", IEEE Trans. Nucl. Sci., Vol.54, no.2, 2007

[11] V. T. Jordanov et G. F. Knoll, "Digital pulse processor using a moving average technique", IEEE Trans. Nucl. Sci., Vol. 40, no. 4, pp. 76-769, 1993.

[12] T. Lakatos, "Adaptative digital signal processing for x-ray spectrometry", Nucl. Instr. and Meth. B, Vol. B47, pp. 30-310, 1990.

[13] A. Georgiev et W. Gast, "Digital pulse processing in high resolution, high throughput gamma-ray spectroscopy", IEEE Trans. Nucl. Sci., Vol. 40, no. 4, pp. 534-536, 1993

[14] N. Petrick et al. , "A fast least squares arrival time estimator for scintillation pulses", IEEE Trans. Nucl. Sci., Vol. 41, no. 4, pp. 758-760, 1994.

[15] Roberto Abbiati, Angelo Geraci, and Giancarlo Ripamonti, "A Weighted least mean squares linear algorithm for energy and occurrence time measurement of pulse", IEEE Trans. Nucl. Sci., Vol. 54, no. 3, pp. 629-634, 2007

[16] G. Ripamonti et A. Geraci, "Towards real time digital pulse processing based on least mean squares algorithms", Nucl. Instr. and Meth. A, Vol. A400, pp. 447-455, 1997

[17] W.W. Moses, S.E. Derenzo, "Prospects for Time Of Flight PET using LSO scintillator", IEEE Trans. Nucl. Sci., Vol. 46, no 3, pp. 474-478, 1999

[18] M. Moszynski et al., "New prospects for Time-of-Flight PET with LSO scintillators", IEEE Trans. Nucl. Sci., Vol. 53, no 5, pp. 2484-2488, 2006

[19] J.S.Huber et al., "Geometry and surface treatment dependence of the light collection from LSO crystals", Nucl. Instr. and Meth. Section A, Vol. 437, no 2-3, pp. 374-380, 1999

[20] T. Szczesniak et al., "A Further study of timing with LSO on XP20D0 for TOF PET", Nucl. Instr. Meth. A, Vol. 54, Issue 5, pp. 1464-1473, 2007

[21] A. Kuhn et al., "Design of a lanthanum bromide detector for time-of-flight PET", IEEE Trans. Nucl. Sci., Vol. 51 (5), pp. 2550-2557, 2004

[22] A. Kuhn, S. Surti, K.S. Shah, J.S. Karp, "Investigation of LaBr3 detector timing resolution", IEEE NSS Conference Record, Vol. 4, 2005

[23] R.F. Post, L.I. Schiff, "Statistical limitations on the resolving time of a scintillation counter", Phys. Rev., Vol. 80, pp. 1113-1120, 1950

[24] M. Kelbert, I. Sazonov, A.G. Wright, "Exact expression for the variance of the photon emission process in scintillation counters", Nucl. Instr. and Meth., A 564, pp. 185-189, 2006

[25] G. Ranucci, "Time statistics of the photoelectron emission process in scintillation counters", Nucl. Instr. and Meth. A Vol 335 (1-2), pp. 121-128, 1993

[26] Y. Shao, "A new timing model for calculating the intrinsic timing resolution of a scintillator detector", Phys. Med. Biol. 52, pp. 1103-1117, 2007

[27] K.Deiters et al., "Properties of the avalanche photodiodes for the CMS electromagnetic calorimeter", Nucl. Instr. and Meth. A, Vol. 453, no. 1-2, pp. 223-226, 2000

[28] I. Brivitch et al., "Avalanche photodiodes now and possible developments", Nucl. Instr. and Meth. A, Vol. 535, pp. 523-527, 2004

[29] M. Kapusta et al., "Avalanche photodiodes in scintillation detection for high resolution PET", IEEE Trans. Nucl. Sci., Vol. 47 (6), pp. 2029-2033, 2000

[30] "CR110 charge sensitive preamplifier application guide", 2006

[31] M. Moszynski et al., "New Photonis XP20D0 photomultiplier for fast timing in nuclear medicine" Nucl. Instr. and Meth. A, Volume 567, Issue 1, pp. 31-35, 2006

[32] F. Druillole et al., "The Analog Ring Sampler: an ASIC for the front-end electronics of the ANTARES neutrino telescope", IEEE. Trans. Nucl. Sci., Vol. 49, no. 3, pp. 1122-1129, 2002